INFLUENCE OF PYRAMIDAL AND SPHERICAL EMBOSSING ON RESIDUAL STRESS DISTRIBUTION AND MAGNETIC MATERIAL PROPERTIES OF NON-ORIENTED ELECTRICAL STEEL

Ines Gilch[1*], Benedikt Schauerte[2], Tobias Neuwirth[3], Simon Sebold[3], Michael Schulz[3], Kay Hameyer[2], Wolfram Volk[1]

[1] Chair of Metal Forming and Casting (*utg*), Technical University of Munich, Germany

[2] Institute of Electrical Machines (IEM), RWTH Aachen, Germany

[3] Heinz Maier-Leibnitz Zentrum (MLZ), Technical University of Munich, Germany

ABSTRACT

Due to inverse magnetostriction, residual stresses in soft magnetic materials deteriorate their magnetic material properties such as magnetizability and iron losses. Hence, in the production of electrical steel components, residual stresses should be avoided to reduce iron losses. Targeted residual stresses enable a local deterioration of magnetic material properties, which can be used to guide magnetic flux in electrical steels. In rotors of synchronous reluctance machines and permanent-magnet synchronous-machines, magnetic flux guidance is required to induce magnetic anisotropy and reduce stray flux. Conventionally, flux barriers are manufactured as cutouts, which diminish the mechanical strength, hence reducing the maximum rotational speed of the rotor. In this work, an alternative design of magnetic flux barriers by embossing induced residual stresses is studied in detail, which allows to increase maximum rotational speed, energy density and efficiency. The functionality of embossed flux barriers depends on the residual stress distribution in the designated area. The embossing geometry and grade of deformation are key parameters to adjust the residual stress distribution. The presented study shows the comparison of spherical and pyramidal embossing geometries focused on the numerically evaluated residual stress distribution as well as the local and global magnetic material properties. The key result is that both embossing force and embossing shape influence the residual stress distribution. At low embossing forces, the increased degree of plastic deformation caused by pyramidal punch facilitates higher compressive residual stresses and magnetic material deterioration compared to the more elastic deformation caused by a spherical punch.

KEYWORDS: Magnetic Flux Barrier, Residual Stress, Embossing, Inverse Magnetostriction

1 INTRODUCTION

The high demand and importance of electro mobility as well as the necessity of energy saving requires more efficient electric drives. One possibility is to increase the energy density of electric drives by applying higher rotational speeds. Among others, typical electric drive topologies for electric vehicles are synchronous reluctance machines (SynRM) and permanent magnet synchronous machines (PMSM) [1]. Both topologies require magnetic flux barriers to guide the magnetic flux in the rotor, reducing stray fluxes or producing a targeted magnetic anisotropy [2]. Magnetic flux barriers are conventionally fabricated by removing the material in areas, where the magnetic flux is undesired. These cutouts result in a filigree rotor construction for example next to the permanent magnets of a PMSM or between flux barriers and close to the sheets edge of SynRM (see Figure 1). The resulting rotor geometry limits the maximum achievable rotational speed, while high rotational speed is desired to increase the energy density of the electric drive [3].

*Ines Gilch, Walther-Meißner-Straße 4, 85748 Garching, Germany, ines.gilch@utg.de

Figure 1: *Schematic rotor construction of typical SynRM.*

A higher mechanical strength and hence rotational speed of the rotor requires an alternative approach for the magnetic flux guidance, as increasing the width of the ridges increases stray flux. The actual research analyzes a production process to locally degrade magnetic material properties of electrical steel to build barriers for the magnetic flux. This phenomenon is known as the *Villari effect* or *inverse magnetostriction*. Higher mechanical stresses reduce the magnetizability of the electrical steel [4].
Earlier publications [5–9] show that embossing induced residual stresses deteriorate the local permeability of electrical steel and can be applied to guide the magnetic flux. In embossed areas, the magnetizability and the local magnetic flux density is reduced whereas in the non-embossed areas a concentration of magnetic flux is observed. Different embossing strategies can influence the properties of the embossed magnetic flux barrier. Figure 2 shows schematically the application of embossed flux barriers on a SynRM, which will be examined in the future.

Figure 2: *Schematic application of embossed magnetic flux barriers to realize the SynRM concept.*

As the mechanical stress distribution in the embossed magnetic flux barriers is essential for their functionality, the influence of the embossing geometry has to be analyzed in more detail. Two different embossing strategies are evaluated. The embossing with a pyramidal embossing punch, which leads to a fast plasticization due to the sharp geometry, is compared to a spherical embossing punch, which shows a higher amount of elastic deformation.
Samples embossed with a pyramidal or spherical punch with an embossing force of 50 N, 100 N or 200 N are evaluated regarding their residual stress state and magnetic material properties. The residual stresses are numerically analyzed by FEM simulation. The magnetizability is measured with a Single Sheet Tester (SST). Neutron Grating Interferometry (nGI) allows the qualitative evaluation of the local magnetic material behavior.

2 METHODS

2.1 EMBOSSING PROCESS

The specimens are fabricated of a non-oriented electrical steel sheet with a silicon content of 2.4 wt-% and a sheet thickness of 0.35 mm. The sample geometry – 10 mm x 60 mm – is spark eroded to have a minimal effect on the magnetic material properties due to the cutting process [10]. The long side of the specimen is oriented parallel to the rolling direction of the sheet material. To enable comparability to previous studies [5–8], the specimen's material, size and orientation is maintained.
The embossing process is conducted as described in [6]. With a single embossing punch, 20 embossing points with a distance of 0.5 mm are induced in a line in the specimen's center perpendicular to the long edge of the specimen, see Figure 3. The first and last embossing point have a distance of 0.25 mm to the sample's edges. The embossing punches are a four-sided pyramid with a tip angle of 136.5° and a spherical punch with a diameter of 1.05 mm. The die is flat.
The embossing process is implemented on a universal testing machine to conduct reproducible experiments. To induce different residual stress distributions the embossing force per embossing point is varied between 50 N, 100 N and 200 N.

2.2 NUMERICAL ANALYSIS OF RESIDUAL STRESS DISTRIBUTION

With a numerical analysis based on the Finite Element Method (FEM) the residual stress distribution in the specimen can be estimated. Due to the specimen's and punch's symmetry, it is sufficient to calculate the half model with the xy-

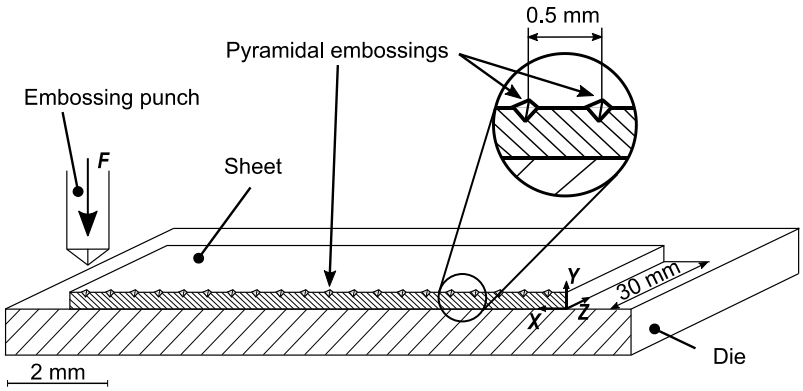

Figure 3: *Schematic illustration of the sequential embossing process with a flat die and a pyramidal punch [6].*

symmetry-plane, shown in Figure 3. The sheet has 69115 linear hexahedral elements of type C3D8R. The elements edge length varies between 0.01 mm (embossed area) and 1 mm (non-embossed area). Based on the measured mechanical properties with the mechanical anisotropy due to the rolling analyzed in [11] and the Hill'48 yield criterion a material model is set up. After the numerical analysis of the sequential embossing process, all boundary conditions except the symmetry condition are removed to allow springback after embossing. Subsequently no external forces act on the specimen and the residual stress distribution can be evaluated.

To evaluate the distribution of residual stresses, the mean stresses over the sheet thickness are simulated. For the application as magnetic flux barrier, a locally restricted increase of residual stresses is favored. Additional to the two-dimensional analysis, the distribution of residual stresses in the cross section of the embossing line, hence the xy-plane, is of high interest.

2.3 MAGNETIC MEASUREMENTS

The influence of embossing induced residual stresses on the magnetic material properties is measured with a Single Sheet Tester (SST) and Neutron Grating Interferometry (nGI). The SST measurements analyze the global magnetic behavior of the specimen. The relative magnetic permeability is evaluated as a measure for the magnetizability. The embossing induced residual stresses reduce the permeability, a higher reduction signifies a better applicability of the embossing strategy in magnetic flux barriers.

The local magnetic material behavior averaged over the sheet thickness can qualitatively be analyzed by nGI. The resulting Dark Field Image (DFI) shows, whether the material is locally weaker (normalized signal < 1) or stronger (normalized signal > 1) magnetized than an unworked reference specimen. The measurement procedures are described in [5, 6, 8] in detail.

3 RESULTS

3.1 RESIDUAL STRESS DISTRIBUTION

The calculated residual stress distributions are evaluated in two different ways. By averaging over the sheet thickness, the mean stress distribution over the specimen area is calculated. Secondly, the comparison of minimum and maximum principal residual stresses in the xy-symmetry-plane show the distribution of tensile and compressive stresses in the sheet's cross section.

Figure 4 presents the distribution of hydrostatic stresses. The differences between the two embossing strategies with spherical and pyramidal punch are very small. Higher embossing forces also increase the area with residual stresses. This can be observed for both punch geometries.

In addition to the hydrostatic stresses, which are a measure for mean stresses, the absolute maximum principal stresses are considered. As tensile and compressive residual stresses have a different impact on the magnetic material properties, in Figure 5 the absolute maximum principal stresses are averaged over the sheet thickness. Similar to the hydrostatic stress distribution the difference between spherical and pyramidal embossings are very small. The influence of embossing force however, is significant and primarily results in larger affected areas. For both stress components, the residual stresses at 50 N embossing force are quite homogeneous. With increasing embossing force, the compressive stresses dominate the area 0 mm <= x <= 5 mm and x >= 9 mm for 200 N. The area of tensile stresses for 200 N is 5 mm <= x <= 9 mm. For 100 N embossing force, the area with dominant tensile stresses is smaller with 7 mm <= x <= 9 mm. This is quite similar for spherical and pyramidal embossing. The variation of compressive and tensile residual stresses across the sheet's width was already observed in [6] and attributed to the sequential embossing process.

*Ines Gilch, Walther-Meißner-Straße 4, 85748 Garching, Germany, ines.gilch@utg.de

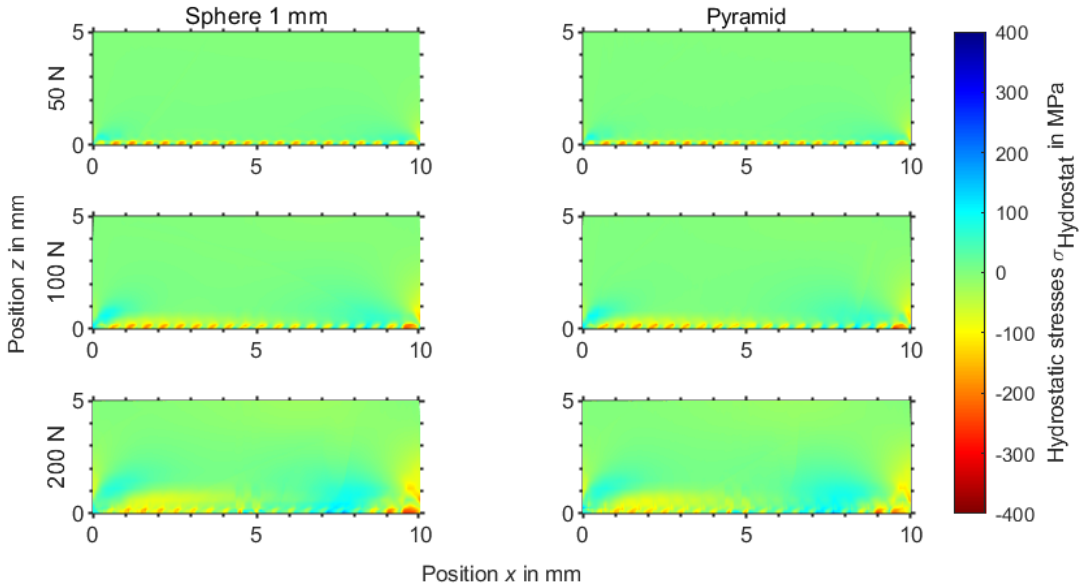

Figure 4: *Mean residual stresses over sheet thickness of pyramidal and spherical embossed specimen and varying embossing force: Hydrostatic stresses.*

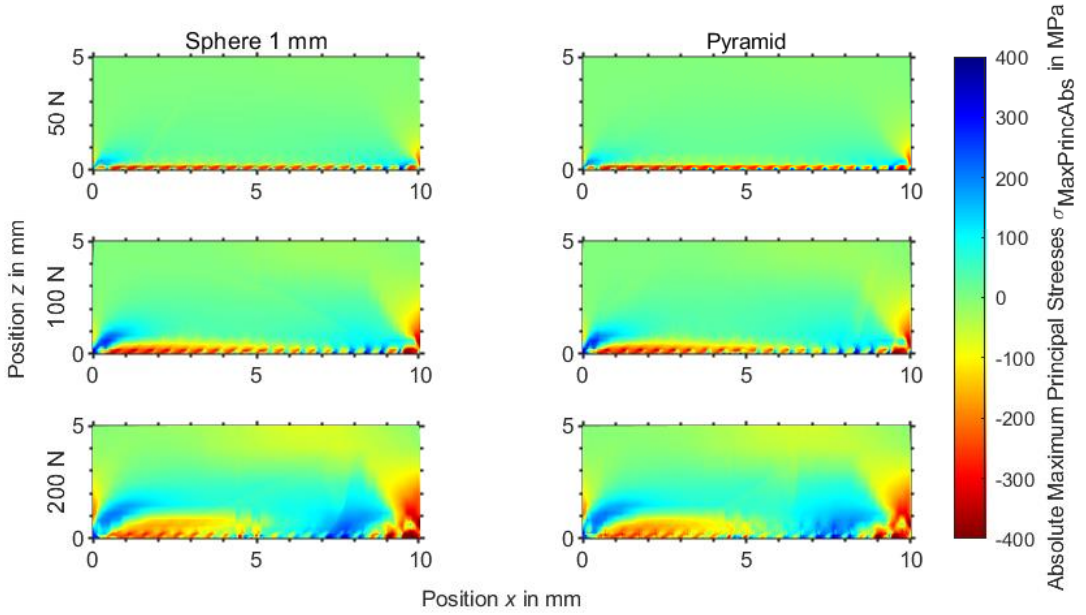

Figure 5: *Mean residual stresses over sheet thickness of pyramidal and spherical embossed specimen and varying embossing force: Absolute Maximum Principal Stresses.*

As the average residual stresses over the sheet thickness show only small variations for both embossing geometries, the residual stress distribution in the symmetry plane of the embossing line is evaluated. To point out the differences, it has been decided to show the distribution of tensile and compressive stresses for the maximum and minimum principal stresses. This allows an assessment of the local maximum spread in residual stresses.

Figure 6 shows the minimum principal stresses. For the pyramidal embossing with 50 N, a larger area with compressive residual stresses can be evaluated compared to the spherical embossing with 50 N. Similar tendency is observed in Figure 7 for the maximum principal stresses. The pyramidal embossing at 50 N still shows larger areas with compressive stresses.

For 100 N embossing force, the differences in Figure 6 are rather in the distribution than in the amount of compressive residual stresses. For the maximum principal stresses, the pyramidal embossing leads to very small areas with high compressive residual stresses. Whereas the

*Ines Gilch, Walther-Meißner-Straße 4, 85748 Garching, Germany, ines.gilch@utg.de

spherical embossing has almost no high compressive residual stresses for maximum principal stresses in the cross section.
An embossing force of 200 N leads to a strongly inhomogeneous stress distribution. As already seen in Figure 4 and Figure 5, the compressive stresses are dominant for x <= 5 mm and x >= 8.5 mm. In between, for minimum principal stresses, a low stress level is observed and for maximum residual stresses, tensile stresses are dominant. Here the differences of pyramidal and spherical embossing are strongly in the distribution of stresses. The pyramidal embossing still shows more compressive stresses in the area of 5 mm <= x <= 8.5 mm whereas far less compressive stresses are evaluated for the spherical embossing.

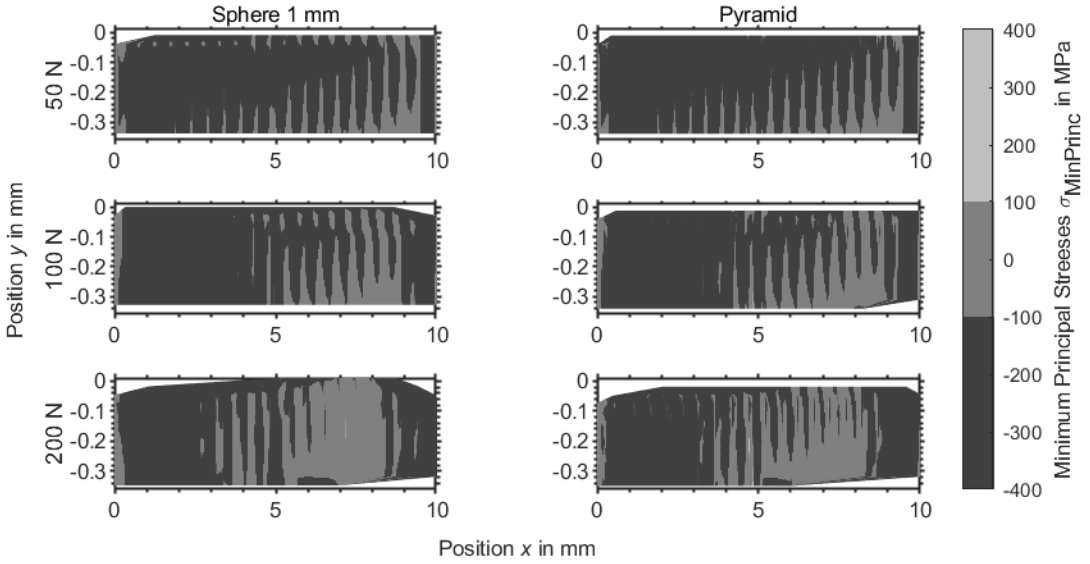

Figure 6: *Residual stresses in symmetry-plane of pyramidal and spherical embossed specimen and varying embossing force: Minimum Principal Stresses.*

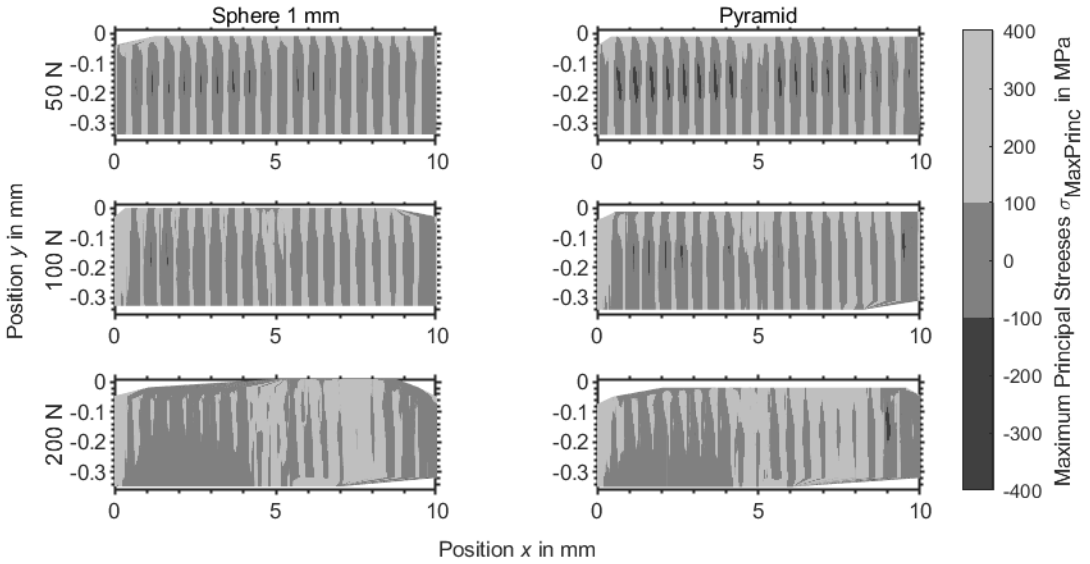

Figure 7: *Residual stresses in symmetry-plane of pyramidal and spherical embossed specimen and varying embossing force: Maximum Principal Stresses.*

3.2 MAGNETIC MATERIAL BEHAVIOR

The global magnetic material behavior is measured with a SST and the relative magnetic permeability is analyzed for the evaluation of the changed magnetic material properties. In Figure 8, the relative permeability of the two embossing geometries is compared for the embossing forces. As reference, a non-embossed specimen is

measured. The embossed samples show a reduction in permeability compared to the reference.
For 50 N embossing force, the magnetic permeability of the pyramidal embossing is strongly decreased. The reduction of permeability of the spherical embossing is only small compared to the reference.
An increase in embossing force to 100 N leads to a further decrease of permeability of the pyramidal embossing. The permeability of the spherical embossed sample is significantly reduced compared to the reference, but not as strong as the pyramidal embossing. The effect is similar to the pyramidal embossing with 50 N.
The highest embossing force with 200 N shows a similar influence of spherical and pyramidal embossing on the magnetic permeability. The permeability values of the pyramidal embossing are only slightly decreased compared to 100 N embossing force. For the spherical embossing, the permeability reduction compared to 100 N is significant.

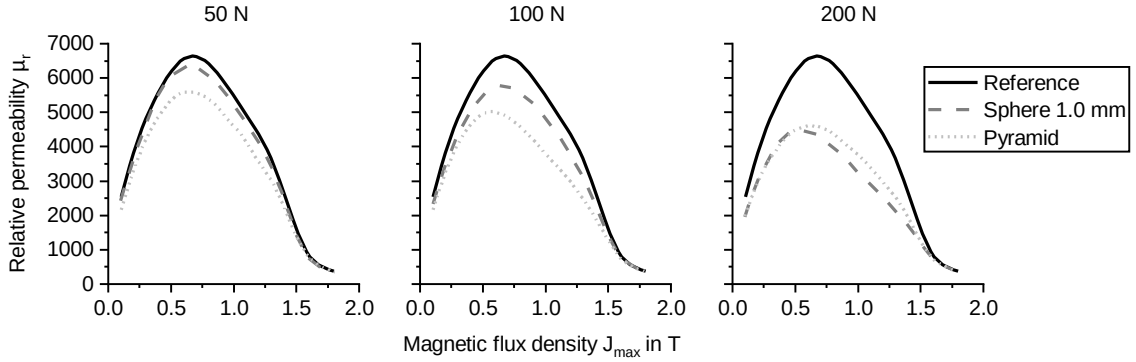

Figure 8: *Magnetic permeability of pyramidal and spherical embossed specimen and varying embossing force.*

Conventional magnetic measurement procedures allow the evaluation of the global magnetic material properties of the specimen. To analyze the influence of the embossing on the local magnetic material behavior, we applied the alternative measurement method Neutron Grating Interferometry (nGI). The resulting Dark Field Images (DFI) for the spherical and pyramidal embossing at 50 N and 200 N embossing force are shown in Figure 9. The results are normalized to a non-embossed reference specimen that allows evaluating whether the embossed specimen is locally stronger or weaker magnetized compared to the reference.
Each result shows clearly the embossing line in the center of the measurement volume. The lower DFI values signify that the sample is weaker magnetized in the area of the embossing points. The embossing lines at 50 N have a small height while the extension of the embossing induced change at 200 N embossing force is significantly larger. For 50 N, the influence of the embossing across the sheet's width is more homogeneous than for 200 N. The pyramidal embossing at 50 N leads to a generally lower DFI when compared to the spherical embossing at 50 N, hence a stronger influence of the pyramidal embossing on the magnetic material properties is detected. For 200 N the general influence of the embossing geometries seems to be quite similar, except the area around x = 8 mm, where a higher magnetization of the spherical embossing in the embossing line is measured compared to the pyramidal embossing.

4 CONCLUSIONS

The numerically analyzed residual stress distributions have to be compared to the measured magnetic material behavior. The magnetic measurements show a strong difference of pyramidal and spherical embossing at 50 N and 100 N, whereas an embossing force of 200 N yields to quite similar global and local magnetizability of spherical and pyramidal embossed specimens. The SST measurements point out, that the embossing with a pyramidal punch and 100 N has a similar effect as the embossing with 200 N and pyramidal or spherical punch. Due to this, the pyramidal embossing with lower embossing force is favorable as it is easier to apply in a manufacturing process.
The mean residual stress distribution over the sheet thickness shows only slight differences of the embossing geometries. Hence, the residual stresses in the plane of embossing are analyzed. This shows a stronger amount of compressive residual stresses for the pyramidal embossing at 50 and 100 N embossing force compared to the spherical embossing.

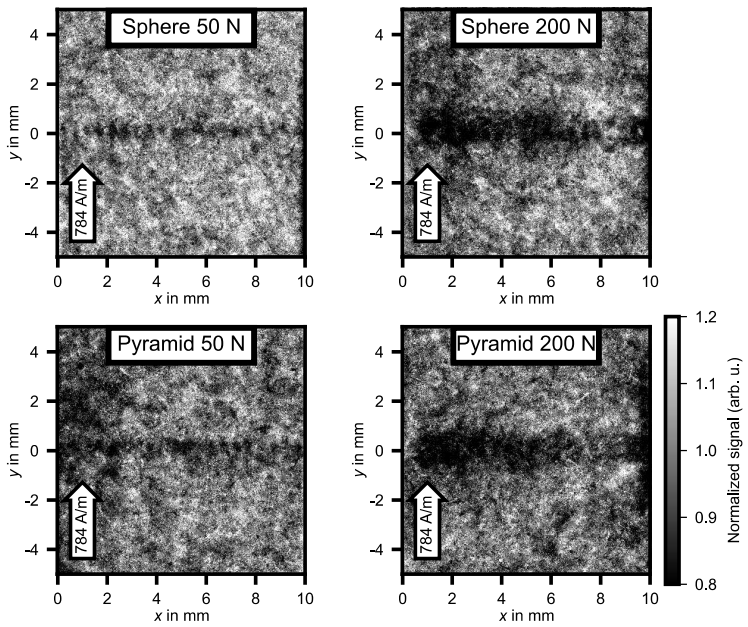

Figure 9: *Scaled Dark Field Image (DFI) of pyramidal and spherical embossed specimen and varying embossing force with applied magnetic field strength of 784 A/m.*

Previous analysis show that compressive residual stresses reduce the magnetizability of electrical steel far stronger than tensile residual stresses [12]. The pyramidal embossing leads already at low embossing forces to a higher amount of compressive residual stresses compared to the spherical embossing geometry. This explains the stronger deterioration of magnetizability for the pyramidal embossing.

Comparing the embossing punch geometries, the tip and the edges of the pyramidal embossing punch lead to locally high stresses, which induce early plastic deformations. For the spherical punch, the deformation is more homogeneous and higher embossing forces are necessary to start the plastic deformation. Hence, the dislocation development at low embossing forces is stronger for the pyramidal embossing because less elastic deformation is possible. At higher embossing forces the difference of embossing geometry decreases, as the amount of elastic compared to plastic deformation shrinks. The performed numerical analysis only shows the residual stress distribution due to embossing induced strains but disregards the amount of dislocations. Dislocations influence the magnetizability of the specimens [4] in addition to the residual stresses.

For further studys, the numerical analysis of the residual stress distribution has to be improved. The influence of mesh density as well as the stress size has to be investigated. The evaluation of stresses is particularly difficult, because of the materials mechanical and magnetic anisotropy combined with resulting anisotropic residual stress distributions at specific magnetization directions. As seen in the evaluation of the residual stresses, the mean values over the sheet thickness are not enough to describe the correlation of residual stress distribution and magnetic material behavior.

To summarize, the embossing induced residual stresses influence the magnetizability of the material locally. This effect depends on the residual stress distribution, which results from the plastic deformation. The pyramidal embossing geometry has therefore a stronger effect on the magnetic behavior at low embossing forces. At embossing force 200 N, the influence of spherical and pyramidal embossing is quite similar but comparable to the effect of the pyramidal embossing at 100 N. Due to all results, the pyramidal embossing at 100 N should be favored, because of lower process forces and more homogeneous residual stress distribution.

In future research, the application of the embossed magnetic flux barriers in real electric drive topologies will be analyzed. Therefore, the correlation between numerically calculated residual stress distributions and magnetic material properties needs to be further evaluated to allow the dimensioning of the embossed magnetic flux barriers.

5 ACKNOWLEDGEMENT

This work was supported by the Deutsche Forschungsgemeinschaft (DFG) in the DFG priority program “SPP2013 “Focused Local Stress Imprint in Electrical Steel as Means of Improving the Energy Efficiency” — 374548845. The results of this work are based upon experiments performed at the ANTARES instrument at Heinz Maier-Leibnitz Zentrum (MLZ), Garching, Germany.

*Ines Gilch, Walther-Meißner-Straße 4, 85748 Garching, Germany, ines.gilch@utg.de

6 AUTHOR CREDITSHIP

IG—conceptualization, specimen manufacturing, investigation (FEA, microhardness), writing; BS—conceptualization, investigation (SST measurements), writing: review and editing; TN—conceptualization, investigation (nGI measurements), writing: review and editing; SS— conceptualization, review and editing; MS—supervision, writing: review and editing; KH—supervision, writing: review and editing; WV—supervision, writing: review and editing.

7 REFERENCES

1. Reddy, P.B., El-Refaie, A.M., Galioto, S., Alexander, J.P.: Design of Synchronous Reluctance Motor Utilizing Dual-Phase Material for Traction Applications. IEEE Transactions on Industry Applications (2017). https://doi.org/10.1109/TIA.2017.2661719
2. Gerada, D., Mebarki, A., Brown, N.L., Gerada, C., Cavagnino, A., Boglietti, A.: High-speed electrical machines: Technologies, trends, and developments. IEEE Transactions on Industrial Electronics (2014). https://doi.org/10.1109/TIE.2013.2286777
3. Chiodetto, N., Mecrow, B., Wrobel, R., Lisle, T.: Electro-Mechanical Challenges in the Design of a High-Speed-High-Power-PMSM Rotor for an Aerospace Application. In: 8912521, pp. 3944–3951 (2019). https://doi.org/10.1109/ECCE.2019.8912521
4. Tumański, S.: Handbook of magnetic measurements. Series in sensors. CRC Press, Boca Raton, FL (2011)
5. Vogt, S., Neuwirth, T., Schauerte, B., Weiss, H.A., Falger, P.M., Gustschin, A., Schulz, M., Hameyer, K., Volk, W.: Extent of embossing-related residual stress on the magnetic properties evaluated using neutron grating interferometry and single sheet test. Production Engineering (2019). https://doi.org/10.1007/s11740-018-0863-7
6. Gilch, I., Neuwirth, T., Schauerte, B., Leuning, N., Sebold, S., Hameyer, K., Schulz, M., Volk, W.: Impact of residual stress evoked by pyramidal embossing on the magnetic material properties of non-oriented electrical steel. Archive of Applied Mechanics (2021). https://doi.org/10.1007/s00419-021-01912-6
7. Schauerte, B., Gilch, I., Neuwirth, T., Sebold, S., Leuning, N., Schulz, M., Volk, W., Hameyer, K.: Alternative Magnetflussführung in Elektromotoren. Forschung im Ingenieurwesen (2021). https://doi.org/10.1007/s10010-021-00493-8
8. Gilch, I., Vogt, S., Neuwirth, T., Schauerte, B., Hameyer, K., Schulz, M., Gustschin, A., Volk, W., Weiss, H.A.: Analysis of Cylindrically and Spherically Embossed Flux Barriers in Non-oriented Electrical Steel. The Minerals, Metals & Materials Series (2021). https://doi.org/10.1007/978-3-030-75381-8_193
9. Schauerte, B., Leuning, N., Vogt, S., Moll, I., Weiss, H., Neuwirth, T., Schulz, M., Volk, W., Hameyer, K.: The influence of residual stress on flux-barriers of non-oriented electrical steel. Journal of Magnetism and Magnetic Materials (2020). https://doi.org/10.1016/j.jmmm.2020.166659
10. Kurosaki, Y., Mogi, H., Fujii, H., Kubota, T., Shiozaki, M.: Importance of punching and workability in non-oriented electrical steel sheets. Journal of Magnetism and Magnetic Materials (2008). https://doi.org/10.1016/j.jmmm.2008.04.073
11. Weiss, H.A., Leuning, N., Steentjes, S., Hameyer, K., Andorfer, T., Jenner, S., Volk, W.: Influence of shear cutting parameters on the electromagnetic properties of non-oriented electrical steel sheets. Journal of Magnetism and Magnetic Materials (2017). https://doi.org/10.1016/j.jmmm.2016.08.002
12. LoBue, M., Sasso, C., Basso, V., Fiorillo, F., Bertotti, G.: Power losses and magnetization process in Fe-Si non-oriented steels under tensile and compressive stress. Journal of Magnetism and Magnetic Materials (2000). https://doi.org/10.1016/S0304-8853(00)00092-5